Hybrid integrated plasmonic-photonic waveguides for on-chip localized surface plasmon resonance (LSPR) sensing and spectroscopy

Maysamreza Chamanzar, Zhixuan Xia, Siva Yegnanarayanan, and Ali Adibi*

School of Electrical and Computer Engineering, Georgia Institute of Technology,Atlanta, GA 30332, USA

*adibi@ece.gatech.edu

Abstract: We experimentally demonstrate efficient extinction spectroscopy of single plasmonic gold nanorods with exquisite fidelity ($SNR > 20dB$) and high efficiency light coupling (e. g., 9.7%) to individual plasmonic nanoparticles in an integrated platform. We demonstrate chip-scale integration of lithographically defined plasmonic nanoparticles on silicon nitride (Si_3N_4) ridge waveguides for on-chip localized surface plasmon resonance (LSPR) sensing. The integration of this hybrid plasmonic-photonic platform with microfluidic sample delivery system is also discussed for on-chip LSPR sensing of D-glucose with a large sensitivity of $\sim 250\ nm/RIU$. The proposed architecture provides an efficient means of interrogating individual plasmonic nanoparticles with large SNR in an integrated alignment-insensitive platform, suitable for high-density on-chip sensing and spectroscopy applications.

OCIS codes: (240.6680) Surface plasmons; (280.1415) Biological sensing and sensors; (220.4241) Nanostructure fabrication; (250.5300) Photonic integrated circuits; (130.2790) Guided waves.

References and links

1. K. Willets and R. Van Duyne, "Localized surface plasmon resonance spectroscopy and sensing," Annu. Rev. Phys. Chem. **58**, 267–297 (2007).
2. I. El-Sayed, X. Huang, and M. El-Sayed, "Surface plasmon resonance scattering and absorption of anti-EGFR antibody conjugated gold nanoparticles in cancer diagnostics: applications in oral cancer," Nano Lett. **5**, 829–834 (2005).
3. A. Haes, W. Hall, L. Chang, W. Klein, and R. Van Duyne, "A localized surface plasmon resonance biosensor: First steps toward an assay for alzheimer's disease," Nano Lett. **4**, 1029–1034 (2004).
4. A. Haes and R. Van Duyne, "A nanoscale optical biosensor: sensitivity and selectivity of an approach based on the localized surface plasmon resonance spectroscopy of triangular silver nanoparticles," J. Am. Chem. Soc. **124**, 10596–10604 (2002).
5. A. Barhoumi, D. Zhang, F. Tam, and N. Halas, "Surface-enhanced Raman spectroscopy of DNA," J. Am. Chem. Soc. **130**, 5523–5529 (2008).
6. A. Gopinath, S. Boriskina, W. Premasiri, L. Ziegler, B. Reinhard, and L. Dal Negro, "Plasmonic nanogalaxies: multiscale aperiodic arrays for surface-enhanced Raman sensing," Nano Lett. **9**, 3922–3929 (2009).
7. K. Kho, U. S. Dinish, A. Kumar, and M. Olivo, "Frequency shifts in SERS for bio-sensing," ACS Nano **6**, 4892-4902 (2012).

#197900 - $15.00 USD Received 19 Sep 2013; revised 21 Nov 2013; accepted 27 Nov 2013; published 18 Dec 2013

8. A. McFarland and R. Van Duyne, "Single silver nanoparticles as real-time optical sensors with zeptomole sensitivity," Nano Lett. **3**, 1057–1062 (2003).
9. G. Raschke, S. Kowarik, T. Franzl, C. Sönnichsen, T. Klar, J. Feldmann, A. Nichtl, and K. Kürzinger, "Biomolecular recognition based on single gold nanoparticle light scattering," Nano Lett. **3**, 935–938 (2003).
10. S. Stranahan and K. Willets, "Super-resolution optical imaging of single-molecule SERS hot spots," Nano Lett. **10** 3777-3784 (2010).
11. E. Ringe, B. Sharma, A.-I. Henry, L. D. Marks, and R. P. Van Duyne, "Single nanoparticle plasmonics," Phys. Chem. Chem. Phys. **15**, 4110–4129 (2013).
12. M. Chamanzar, M. Soltani, B. Momeni, S. Yegnanarayanan, and A. Adibi, "Hybrid photonic surface-plasmon-polariton ring resonators for sensing applications," Appl. Phys. B-Lasers O. **101**, 263–271 (2010).
13. M. Chamanzar and A. Adibi, "Hybrid nanoplasmonic-photonic resonators for efficient coupling of light to single plasmonic nanoresonators," Opt. Express **19**, 22292–22304 (2011).
14. M. Fvrier, P. Gogol, A. Aassime, R. Mgy, C. Delacour, A. Chelnokov, A. Apuzzo, S. Blaize, J.-M. Lourtioz, and B. Dagens, "Giant coupling effect between metal nanoparticle chain and optical waveguide," Nano Lett. **12**, 1032–1037 (2012).
15. F. B. Arango, A. Kwadrin, and A. F. Koenderink, "Plasmonic antennas hybridized with dielectric waveguides," ACS Nano **6**, 10156–10167 (2012).
16. X. Yang, A. Ishikawa, X. Yin, and X. Zhang, "Hybrid photonic-plasmonic crystal nanocavities," ACS Nano **5**, 2831–2838 (2011).
17. S. Boriskina and B. Reinhard, "Spectrally and spatially configurable superlenses for optoplasmonic nanocircuits," P. Nat. Acad. Sci. **108**, 3147–3151 (2011).
18. V. R. Dantham, S. Holler, C. Barbre, D. Keng, V. Kolchenko, and S. Arnold, "Label-free detection of single protein using a nanoplasmonic-photonic hybrid microcavity," Nano Lett. **13**, 3347–3351 (2013).
19. M. A. Santiago-Cordoba, M. Cetinkaya, S. V. Boriskina, F. Vollmer, and M. C. Demirel, "Ultrasensitive detection of a protein by optical trapping in a photonic-plasmonic microcavity," J. Biophotonics **5**, 629–638 (2012).
20. L. Feng, D. Van Orden, M. Abashin, V. Lomakin, and Y. Fainman, "Nanoscale optical field localization by resonantly focused plasmons," in "International Quantum Electronics Conference," (Optical Society of America, 2009).
21. J. Kim, "Joining plasmonics with microfluidics: from convenience to inevitability," Lab Chip **12**, 3611–3623 (2012).
22. Y. Zhang, Y. Tang, Y.-H. Hsieh, C.-Y. Hsu, J. Xi, K.-J. Lin, and X. Jiang, "Towards a high-throughput label-free detection system combining localized-surface plasmon resonance and microfluidics," Lab Chip **12**, 3012–3015 (2012).
23. H.-I. Peng, C. M. Strohsahl, and B. L. Miller, "Microfluidic nanoplasmonic-enabled device for multiplex DNA detection," Lab Chip **12**, 1089–1093 (2012).
24. E. Shah Hosseini, S. Yegnanarayanan, A. Atabaki, M. Soltani, and A. Adibi, "High quality planar silicon nitride microdisk resonators for integrated photonics in the visible wavelength range," Opt. Express **17**, 14543–14551 (2009).
25. X. Fan, I. White, S. Shopova, H. Zhu, J. Suter, and Y. Sun, "Sensitive optical biosensors for unlabeled targets: a review," Anal. Chim. Acta. **620**, 8–26 (2008).
26. M. E. Mahmoud, M. Chamanzar, A. Adibi, and M. El-Sayed, "Effect of the dielectric constant of the surrounding medium and the substrate on the surface plasmon resonance spectrum and sensitivity factors of highly symmetric systems; silver nanocubes," J. Am. Chem. Soc. **134**, 6434–6442 (2012).
27. J. Anker, W. Hall, O. Lyandres, N. Shah, J. Zhao, and R. Van Duyne, "Biosensing with plasmonic nanosensors," Nat. Mater. **7**, 442–453 (2008).
28. D. Duffy, J. McDonald, O. Schueller, and G. Whitesides, "Rapid prototyping of microfluidic systems in poly (dimethylsiloxane)," Anal. Chem. **70**, 4974–4984 (1998).
29. P. K. Jain, K. S. Lee, I. H. El-Sayed, and M. A. El-Sayed, "Calculated absorption and scattering properties of gold nanoparticles of different size, shape, and composition: applications in biological imaging and biomedicine," J. Phys. Chem. B **110**, 7238–7248 (2006).
30. T. Shoji, T. Tsuchizawa, T. Watanabe, K. Yamada, and H. Morita, "Low loss mode size converter from 0.3 μm square Si wire waveguides to singlemode fibres," Electron. Lett. **38**, 1669–1670 (2002).
31. B. Momeni, E. Hosseini, and A. Adibi, "Planar photonic crystal microspectrometers in silicon-nitride for the visible range," Opt. Express **17**, 17060–17069 (2009).
32. M. Chamanzar, B. Momeni, and A. Adibi, "Compact on-chip interferometers with high spectral sensitivity," Opt. Lett. **34**, 220–222 (2009).
33. C. A. Barrios, B. Snchez, K. B. Gylfason, A. Griol, H. Sohlstrm, M. Holgado, and R. Casquel, "Demonstration of slot-waveguide structures on silicon nitride / silicon oxide platform," Opt. Express **15**, 6846-6856 (2007) .
34. D. Yin, H. Schmidt, J. Barber, and A. Hawkins, "Integrated ARROW waveguides with hollow cores," Opt. Express **12**, 2710-2715 (2004).
35. R. Charbonneau, N. Lahoud, G. Mattiussi, and P. Berini, "Demonstration of integrated optics elements based on long-ranging surface plasmon polaritons," Opt. Express **13**, 977-984 (2005).

#197900 - $15.00 USD Received 19 Sep 2013; revised 21 Nov 2013; accepted 27 Nov 2013; published 18 Dec 2013

1. Introduction

Plasmonic nanoparticle LSPR modes arise from collective oscillations of electrons on the surface of metal nanoparticles excited by light. The very localized nature of these modes results in ultrahigh field enhancements, suitable for effective light-matter interaction in applications such as LSPR sensing and spectroscopy based on surface enhanced Raman scattering (SERS) [1–7]. The resonance wavelengths of LSPR modes are very sensitive to the refractive index of the local environment surrounding nanoparticles, forming the basis for LSPR sensing, where the change of refractive index near plasmonic nanoparticles is determined based on the LSPR wavelength shift [1]. While interrogation of single or a few plasmonic nanoparticles has always been of great interest in LSPR sensing [8–11], it has been challenging to couple light to the LSPR modes of individual plasmonic nanoparticles using conventional free-space excitation techniques (e. g., using an objective lens.) This is because of the order-of-magnitude difference between the diffraction-limited spot size of a focused light (i.e., $\lambda/2NA$, λ being the wavelength, and NA the numerical aperture) and the cross section of nanoparticle. Because of this low coupling efficiency, usually intricate test equipment such as dark-field microscopes equipped with cooled CCD detectors are required to perform single nanoparticle LSPR sensing [8,9]. Recent developments in on-chip sensing applications employing advancements in nanotechnology, photonics, fluidics, and biochemistry have had profound impacts on medicine and pharmaceutical industry by enabling a paradigm shift in health care distribution through providing fast, low-cost, and very accurate sensing capabilities at point-of-care to a much wider user base. Plasmonic nanoparticles have a strong potential for facilitating effective light interaction with small bio and chemical molecules in sensing applications [11]. This great potential can be utilized in practice, specially if individual nanoparticles can be interrogated efficiently in an integrated platform without requiring bulky and expensive lab equipment. To utilize the potentials of plasmonic nanoparticles for practical on-chip sensing applications, it is crucial to devise methods and mechanisms for performing extinction spectroscopy with large signal-to-noise ratio (SNR) and in an alignment-insensitive arrangement. Therefore, it is highly desirable to incorporate plasmonic nanoparticles into an integrated platform so that they can be efficiently interrogated and interact with target molecules. In view of these requirements, several recent research efforts have been dedicated to incorporating plasmonics into an integrated platform and solving the problem of low coupling efficiency in free space. In our previous works, we have shown efficient coupling of propagating surface plasmon modes and also LSPR modes with dielectric photonic microresonator whispering gallery modes. This approach takes advantage of the high quality factor (high-Q) of photonic microresonator modes as well as the field enhancement and large sensitivity of plasmonic modes [12, 13]. The coupling of a nanoparticle chain waveguide and also nanoantennas with dielectric waveguides is discussed elsewhere [14, 15]. A subwavelength hybrid photonic-plasmonic crystal nanocavity has been demonstrated, where photonic crystal modes are hybridized with plasmonic modes to form a deep subwavelength and at the same time high-Q hybrid mode [16]. A reconfigurable optoplasmonic superlens has also been demonstrated based on the combination of photonic microspheres and plasmonic nanospheres for enhancing dipole radiative rates [17]. Such structures have been recently used for the label-free detection of single proteins with exquisite detection limits [18, 19]. It has also been demonstrated that a nanoscale antenna can be used to focus the propagating mode of a silicon waveguide to a sub-diffraction-limit spot [20]. The integration of plasmonic structures with microfluidics is also discussed recently for sensing applications [21–23]. In this paper, we demonstrate a hybrid plasmonic-photonic waveguide structure integrated with microfluidics in which light can be efficiently coupled to the LSPR mode of plasmonic nanoparticles over the entire band of the LSPR mode, thus improving the signal-to-noise ratio (SNR) and providing the possibility of single nanoparticle extinction (absorption and scattering) spectroscopy, as

#197900 - $15.00 USD Received 19 Sep 2013; revised 21 Nov 2013; accepted 27 Nov 2013; published 18 Dec 2013

well as efficient on-chip LSPR sensing.

2. Hybrid plasmonic-photonic LSPR sensor structure

The schematic of the hybrid plasmonic-photonic structure is shown in Fig. 1. It consists of a silicon nitride (Si_3N_4) ridge waveguide integrated with a lithographically defined gold nanorod on top. Silicon nitride is used as the material for the waveguide, since it is transparent over a large spectral range from visible to infrared, and at the same time has a relatively large refractive index [24]. The Si_3N_4 waveguide is realized on a silicon dioxide (SiO_2) substrate on a Si handle layer. The photonic waveguide with a cross section of ($w \times h$) supports a quasi-transverse electric mode (TE-like, i.e., with the major transverse component of the electric field along the width of the waveguide) over a spectral range that spans the entire resonance band of the plasmonic nanoparticle. The ridge waveguide guides light and the evanescent tail of the guided mode excites the plasmonic nanoparticle LSPR mode. The plasmonic nanoparticle considered in this paper is a gold nanorod with dimensions of ($d_1 \times d_2 \times t$) as shown in Fig. 1, where t is the thickness of the gold nanorod. The radius of curvature of the nanorod is half of its width, i.e., ($\frac{d_2}{2}$). Although we have considered a gold nanorod as the plasmonic nanoparticle, other types of nanoparticles can be used in the same hybrid structure and the design, analysis, and fabrication will follow the same procedure. The fraction of input power that is coupled to the LSPR mode is absorbed or scattered by the nanoparticle. The ratio of scattering to absorption depends on the scattering and absorption cross sections of the plasmonic nanoparticle determined by its geometry and its location on the waveguide.

In any refractive index sensing scenario based on a resonance shift, the detection limit, defined as the minimum amount of detectable analyte, depends on the sensitivity, resonance linewidth, and SNR [25]. The sensitivity, defined as the shift of resonance for a unit change of refractive index, is desired to be as large as possible [25]. The resonance linewidth is desired to be as small as possible, and the SNR is desired to be as large as possible. The sensitivity and the linewidth are mostly determined by the design of the nanoparticle and the SNR depends on the excitation coupling efficiency as well as the detection mechanism [26, 27].

Using the proposed hybrid plasmonic-photonic waveguide structure, the extinction of single gold nanorods can be measured with high efficiency and very large SNR. This structure is alignment insensitive, and once the plasmonic nanoparticles are fabricated in the optimal locations

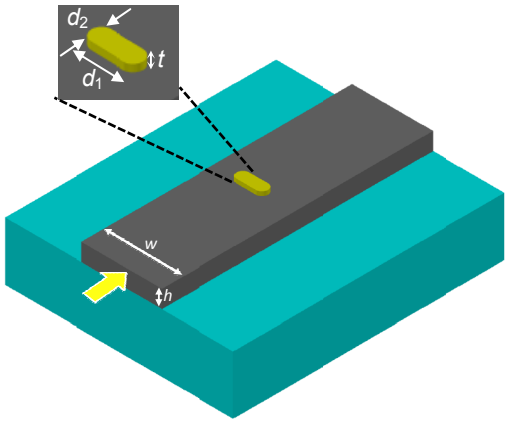

Fig. 1. Schematic of the hybrid plasmonic-photonic structure consisting of a Si_3N_4 ridge waveguide integrated with a plasmonic nanoparticle. The guided mode travelling along the waveguide can excite the LSPR mode of the plasmonic nanoparticle.

#197900 - $15.00 USD Received 19 Sep 2013; revised 21 Nov 2013; accepted 27 Nov 2013; published 18 Dec 2013

on the surface of Si_3N_4 waveguides, the excitation of LSPR modes only requires launching of light into the waveguides. The nearfield interaction of the nanoparticle LSPR mode with the surrounding medium is translated to a change in the output transmission spectrum of the waveguide, and therefore interrogation of plasmonic nanoparticles can be done through transmission measurement at the output of the waveguide, and it does not require bulky and alignment-sensitive microscopes to locate and measure plasmonic nanoparticles.

Our detailed theoretical investigations show that the waveguide dimensions should be designed small enough so that a large coupling can be achieved. However, when the waveguide cross section is decreased below a certain point (i.e., 350 $nm \times 200$ nm), the waveguide mode cuts off over the nanoparticle resonance bandwidth. In practice, however, the waveguide propagation loss increases when the waveguide dimensions are decreased since the mode spreads out further and the effect of scattering loss from sidewall imperfections becomes more pronounced. This added loss makes waveguides with close-to-cut-off operation impractical. Based on all these considerations, the dimensions of the waveguide are chosen to be 865 $nm \times 200$ nm, a close to optimal yet practical design based on the quality of our fabrication. The distance between the waveguide and the nanoparticle determines the coupling strength. Since the nanoparticle quality factor (Q) is very low, the coupling from the waveguide to nanoparticle is always in the undercoupled regime and the optimum case is when the nanoparticle sits directly on the waveguide surface. As we will discuss in the next section, to fabricate the plasmonic nanoparticle on the waveguide, using a thin adhesion layer between the gold nanoparticle and the silicon surface is inevitable in our fabrication process. The adhesion layer degrades the coupling efficiency and should be kept as thin as possible.

3. Fabrication and implementation

Fabrication of the hybrid structure starts with a substrate consisting of a 200 nm stoicheometric Si_3N_4 layer deposited using low-pressure chemical vapor deposition (LPCVD) method on a 3.8 μm thermally grown SiO_2 on a silicon handle wafer. The fabrication procedure as outlined in Fig. 2 involves two steps of electron-beam lithography (EBL). In the first step of EBL, plasmonic nanoparticle patterns are defined in a Polymethyl methacrylate (PMMA) resist with a thickness of 120 nm. Then a 3 nm layer of Titanium (Ti) is deposited using a CHA electron-beam evaporator at a pressure of 3×10^{-7} Torr followed by 27 nm of gold (Au) at a pressure of 2×10^{-7} Torr. Then a lift-off procedure is carried out and the plasmonic nanoparticles are realized on the Si_3N_4 film. The thickness of the Ti/Au nanoparticles is then verified using precise atomic force microscopy (AFM) measurements. In the next step, ZEP520A is spun on the substrate to a thickness of 500 nm, and a second step of EBL is carried out to define the Si_3N_4 wavegiude pattern. Finally, reactive ion etching (RIE) is used to etch the Si_3N_4 film and realize the waveguide. A mixture of 50 $sccm$ of CHF_3 gas and 5 $sccm$ of O_2 is used with a source power of 175 W in an Oxford RIE machine to achieve an average etch rate of $54nm/min$. The alignment between the two steps of EBL is very critical. We use global cross marks as well as chip marks to minimize the alignment error between the two steps of lithography. The advantage of first fabricating the plasmonic layer is that the alignment marks can be realized in the same step with the nanoparticles, thus minimizing the required number of lithography steps and the associated accumulative registration errors. The registration error between the two steps of lithography has always been less than 15 nm (measured over more than 100 different fabrication runs). The scanning electron micrograph (SEM) of an exemplary hybrid structure consisting of a gold nanorod and a Si_3N_4 ridge waveguide is shown in Fig. 3.

In the next step, microfluidic channels and reservoirs are integrated with the hybrid structure. The microfluidic channels are realized in Polydimethylsiloxane (PDMS) using a standard molding procedure on a SU-8 mold [28]. Microfluidic channels realized in PDMS have cross

#197900 - $15.00 USD Received 19 Sep 2013; revised 21 Nov 2013; accepted 27 Nov 2013; published 18 Dec 2013

sectional dimensions of ($25\ \mu m \times 800\ \mu m$) with input/output reservoirs each with a radius of 1 mm. The PDMS microfluidic bottom surface and the Si_3N_4 top surface are treated with oxygen plasma and aligned and bonded together. It is believed that silanol ($Si-OH$) groups form on the surface of PDMS when exposed to oxygen plasma. When the surface of Si_3N_4 is exposed to oxygen plasma, hydroxyl groups form on the surface. When the two surfaces are brought into physical contact, strong $Si-O-Si$ bonds form. Therefore, the channels and reservoirs are strongly sealed. Activation of the surface of PDMS is very sensitive to oxygen plasma parameters. If the oxygen plasma is very weak, the density of formed hydroxyl groups will be low, and the bonding surface area will be small, resulting in leakage from the channels. On the other hand, if the oxygen plasma is too strong, the polymer chain can be damaged, again resulting in poor bonding. Our optimized oxygen plasma parameters on an Oxford RIE tool for a strong, high yield, and repeatable bonding process are as follows; $power = 60\ W, pressure = 30\ mTorr,\ time = 12\ sec$. The image of an integrated microfluidic channel bonded to a hybrid Si_3N_4 structure is shown in Fig. 4. Following the microfluidic integration, the inlet and outlet tubings are connected to the input and output reservoirs, respectively.

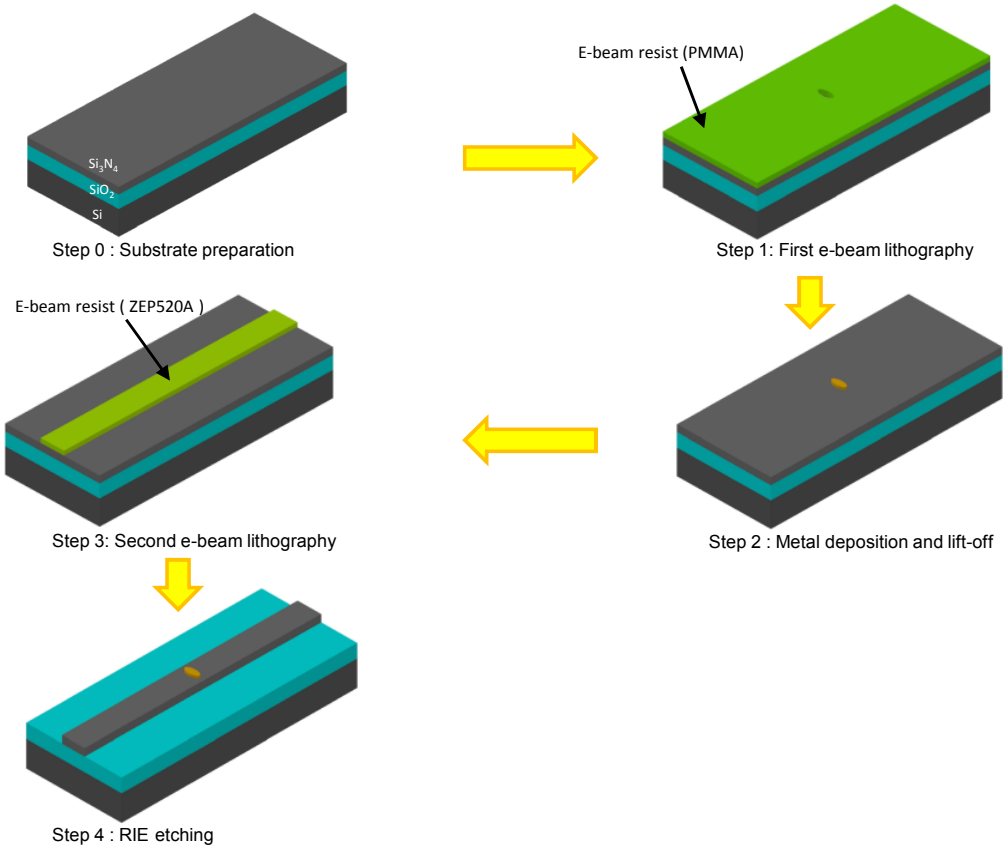

Fig. 2. Fabrication process flow for the hybrid plasmonic-photonic waveguide structure involving two steps of EBL. In the first step, the plasmonic nanoparticle pattern is defined, and then metals consisting of 3 nm Ti and 27 nm Au are deposited, followed by a lift-off procedure. In the next step of lithography, Si_3N_4 ridge waveguide pattern is defined and subsequently etched using RIE.

#197900 - $15.00 USD Received 19 Sep 2013; revised 21 Nov 2013; accepted 27 Nov 2013; published 18 Dec 2013

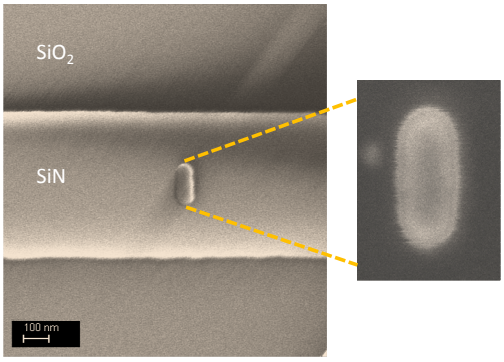

Fig. 3. Scanning electron micrograph (SEM) of an exemplary hybrid plasmonic-photonic waveguide consisting of a gold nanorod and a Si_3N_4 ridge waveguide.

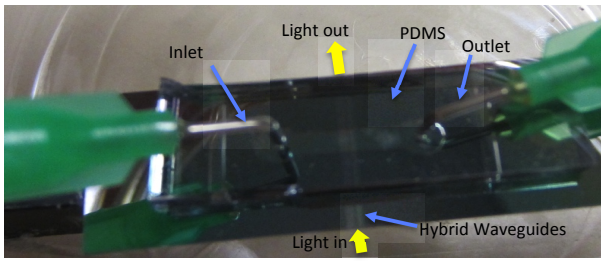

Fig. 4. A PDMS microfluidic system integrated with a Si_3N_4 chip consisting of an array of hybrid waveguides. PDMS is punched on the reservoirs for the insertion of inlet and outlet tubes. The direction of fluid flow is perpendicular to the light travel direction in the waveguides.

4. Experiment

4.1. Optical characterization

To characterize the hybrid on-chip LSPR sensor structure, we use the optical setup that is schematically illustrated in Fig. 5. A supercontinuum broadband laser source (SuperK Compact, NKT Photonics) spanning a wavelength range of $500-1800$ *nm* is butt-coupled to the waveguide through a focusing achromatic input lens. The waveguide output light is collected using a lens and is coupled to an Ocean Optics (USB 2000+) spectrometer. In addition to measuring the LSPR extinction spectrum at the waveguide output, the top microscope assembly is used to image the top surface to monitor the hybrid plasmonic-photonic sensor from top either in the darkfield or the brightfield mode.

The extinction of a plasmonic nanoparticle in this hybrid structure can be obtained according to Eq. 1 by measuring the waveguide output transmission, where the subscripts $''Sample''$ and $''Ref''$ refer to a hybrid waveguide structure with a gold nanorod and the same waveguide without a gold nanorod, respectively. D in Eq. 1 refers to the dark background measurement at the waveguide output, when the input source is blocked.

$$Extinction = -10log(\frac{Trans_{Sample}(\lambda)-D}{Trans_{Ref}(\lambda)-D}), \quad (1)$$

Figure 6(a) shows the normalized measured extinction of different gold nanorods (each curve is normalized to its corresponding maximum), all having a thickness of 27 *nm* and a width of

#197900 - $15.00 USD Received 19 Sep 2013; revised 21 Nov 2013; accepted 27 Nov 2013; published 18 Dec 2013

57 *nm* and varying lengths, fabricated on different Si_3N_4 waveguides with identical dimensions ($w = 865$ *nm* and $h = 200nm$). The integration time in all of the measurements was only 2 *sec* and the source power was attenuated using a variable optical density filter to a low power spectral density of -54 dBm/nm before coupling to the chip. This shows that the coupling efficiency is so large that with a room-temperature detector, a very low input power, and only 2 *sec* integration time, the extinction of plasmonic gold nanorods can be measured easily.

It can be seen from Fig. 6(a) that the resonance wavelength of the nanorod LSPR mode red-shifts as the aspect ratio of the nanorod is increased. The non-normalized extinction spectrum of the gold nanorod with a length of 96 *nm* is shown in Fig. 6(b). This extinction spectrum shows the power removed from the input at each wavelength by the plasmonic nanoparticle. The coupling efficiency, defined as the ratio of the input power coupled to the plasmonic nanoparticle LSPR mode, can be obtained from the extinction LSPR spectrum peak at the resonance wavelength. The SNR can be obtained by measuring the extinction spectrum several times and using the average peak amplitude of the LSPR extinction spectrum as the signal and the standard deviation of the ensemble at the resonance wavelength as the noise. The coupling efficiency and the SNR for all of the hybrid structures discussed in Fig. 6(a) are summarized in Table 1, where it can be seen that the coupling efficiency and the SNR are very large in each case.

Table 1. Coupling efficiency and SNR for different gold nanorods in the hybrid platform.

Gold NanoRods	Coupling Efficiency(%)	Signal-to-noise-ratio (SNR) (dB)
$71 \times 56 \times 27$ *nm*	2.95	15.7
$93 \times 56 \times 27$ *nm*	3.32	19.33
$96 \times 56 \times 27$ *nm*	7.18	20.2
$110 \times 56 \times 27$ *nm*	8.16	20.7
$114 \times 56 \times 27$ *nm*	9.7	24.64

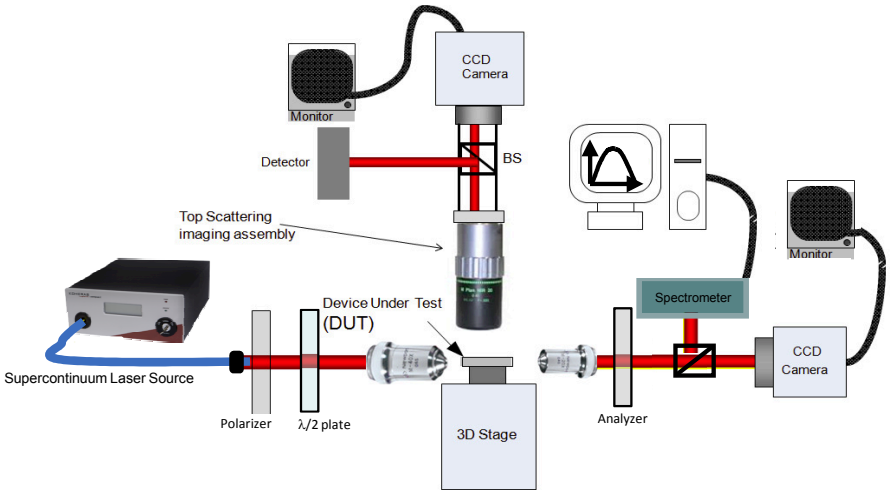

Fig. 5. Schematic of the characterization setup including a supercontinuum laser source and a spectrometer. Light is polarized and then butt-coupled to the input waveguide through a focusing achromatic lens. The waveguide output port is imaged to the entrance slit of a spectrometer. The top microscope assembly can either be used for brightfield or darkfield imaging and scattering measurements.

#197900 - $15.00 USD Received 19 Sep 2013; revised 21 Nov 2013; accepted 27 Nov 2013; published 18 Dec 2013

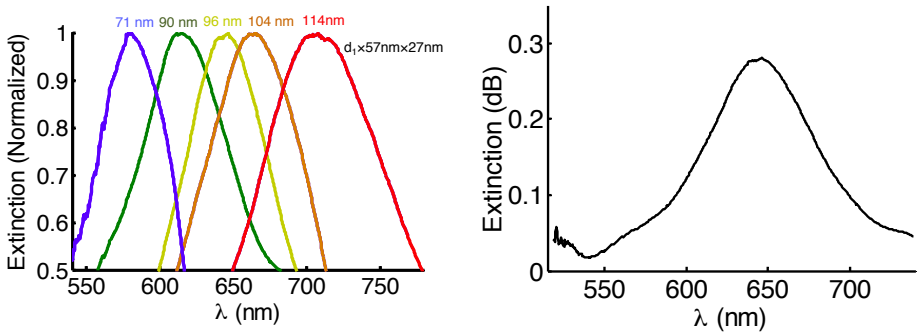

(a) (b)

Fig. 6. (a) Normalized extinction spectrum for different gold nanorods fabricated on different Si_3N_4 waveguides with identical dimensions of 865 $nm \times 200$ nm. All of the nanorods have a thickness of 27 nm and a width of 57 nm, with different lengths (d_1), indicated on each curve. By increasing the length of the gold nanorod, the resonance wavelength redshifts. (b) The extinction spectrum of the single gold nanorod with a length of 96 nm.

To the best of our knowledge, this is the first experimental demonstration of the possibility of coupling light to single nanoparticles with such large coupling efficiencies, as high as 9.7%, in an integrated on-chip platform. As mentioned earlier, the detection limit in LSPR refractive index sensing depends on the SNR; and SNR is directly proportional to the power coupling efficiency. In fact, the traditional assumption of having an input plane wave in free space to excite plasmonic nanoparticles implicitly means that the input power is infinite, which is not the case in practice. In the case of free-space coupling to a plasmonic nanoparticle, the excitation beam with a finite power will have maximum intensity when the beam is focused on the nanoparticle down to the diffraction limit. For example, as an approximate estimation of the coupling efficiency in free space, we can consider a tightly focused (2 μm) beam at the wavelength of 785 nm impinging on a gold nanorod with the polarization state aligned with the nanorod longer axis. The gold nanorod extinction coefficient depends on its shape and size; and it is on the order of $10^{-14} m^2$ [29]. Therefore, the estimated power coupling efficiency is about 0.1% using free-space coupling. It can be seen that our experimentally measured coupling efficiency of 9.7% is about two orders of magnitude better than that of free-space coupling using a lens, and this opens up potentials for the proposed device to be used as a practical on-chip LSPR sensor. The integration of plasmonic nanoparticles with on-chip photonic devices not only provides a robust, alignment-insensitive, and ultracompact platform for on-chip LSPR sensors, but also it has the potential to improve the coupling efficiencies beyond what is possible using free-space optics due to the nearfield interaction between guided modes and the LSPR mode of the plasmonic nanoparticle. Here, based on close-to-optimal yet practical waveguide and plasmonic nanoparticle dimensions, we have been able to achieve coupling efficiencies ranging from 3% up to 9.7%, experimentally. It should be noted that the reported coupling efficiencies are calculated as the power coupled to the nanoparticles divided by the power propagating in the waveguide. This coupling efficiency must be multiplied by the efficiency of light coupling from outside the chip (e. g., from a fiber or a lens) to the waveguide to obtain the overall coupling efficiency to a single nanoparticle from the source. The optimization of insertion loss for coupling of light to on-chip waveguides has been a topic of extensive recent research. For example, it is shown that by using an inverse tapered waveguide at the input, large coupling efficiencies and very low input coupling losses (less than 0.8 dB) can be achieved [30].

#197900 - $15.00 USD Received 19 Sep 2013; revised 21 Nov 2013; accepted 27 Nov 2013; published 18 Dec 2013

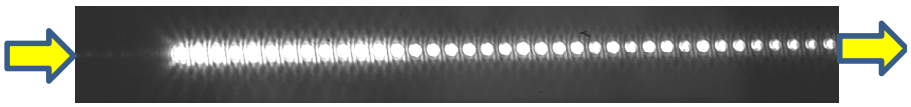

Fig. 7. Darkfield scattering image of an array of identical plasmonic gold nanorods of dimensions $96 \times 57 \times 27$ *nm* integrated with a Si_3N_4 waveguide measured from top.

Arrays of plasmonic nanoparticles with different or similar resonance wavelengths can also be realized on a single waveguide, where they can be excited simultaneously. The top-view darkfield scattering image of an array of plasmonic gold nanorods with identical dimensions of $96 \times 57 \times 27$ *nm* integrated on a single 865 *nm* $\times$ 200 *nm* Si_3N_4 waveguide is shown in Fig. 7. This array is excited using the supercontinuum broadband laser source over the bandwidth of the LSPR resonance. It can be seen that the light from the waveguide is coupled to the LSPR mode of individual plasmonic nanorods and the scattering intensity is reduced as the light propagates along the array in the waveguide. The distance between adjacent nanorods is 11 μm so that the coupling between the nanorods is minimized and also the array does not act as a Bragg reflector at the resonance wavelength of the plasmonic nanorods. The extinction of this array consisting of 40 nanorods is 94% at the output of the waveguide. The use of arrays of plasmonic nanoparticles integrated with photonic waveguides results in higher SNR compared to hybrid structures consisting of single nanoparticles and also provides a larger available volume for light interaction with target molecules. However, all these benefits come at the cost of a larger overall device size and also a broadened lineshape because the nanoparticles cannot be fabricated exactly identical.

4.2. Localized surface plasmon resonance (LSPR) sensing demonstration

To demonstrate the application of the proposed hybrid structure as an on-chip LSPR sensor, we used D-glucose (dextrose) as the test analyte, which is the most abundant isomer of glucose. Dextrose ($C_6H_{12}O_6$) solutions are prepared at different concentrations, and are first characterized using a commercial refractometer to obtain the refractive index associated with each concentration at 20°C as the calibration data. The measurements are repeated multiple times to ensure the accuracy of the calibration data. The results are shown in Fig. 8. The linear regression fit reveals the relation between the concentration of dextrose and the refractive index as $n = 0.16[C] + 1.334$, with a coefficient of determination $R^2 = 0.99$.

To perform the sensing experiments, deionized (DI) water is pumped through the microfluidic channels and the LSPR extinction spectrum is measured as the baseline. Then, dextrose solutions of different concentrations are pumped through the microfluidic channel at the rate of 100 μL/*min*, and the shift of the LSPR peak wavelength is measured with respect to the LSPR peak wavelength for deionized (DI) water. After each sensing step, the channel is completely washed with DI water for 1 hour to make sure that no residue of dextrose is left on the sample, and that the sensor response is returned to the DI water baseline. As an example, in Fig. 9, the LSPR spectrum of a device consisting of 96 $\times 57 \times 27$ *nm* gold nanorods integrated with a 865 *nm* $\times$ 200 *nm* Si_3N_4 waveguide is shown for a dextrose solution of 8% concentration. Similar LSPR extinction spectra of the device for DI water are also shown in Fig. 9 before dextrose measurement and after complete washing of the 8% solution. It can be seen that the introduction of dextrose causes 3 *nm* resonance shift. The extinction spectrum due to DI water measured after the introduction of the dextrose solution matches well with that due to DI water baseline (before the introduction of dextrose solution). This shows that the sensor response is well reversible. The second DI water measurement is carried out 1 hour after the first measurement. The agreement between the two results shows the stability of the on-chip LSPR sensor.

#197900 - $15.00 USD Received 19 Sep 2013; revised 21 Nov 2013; accepted 27 Nov 2013; published 18 Dec 2013

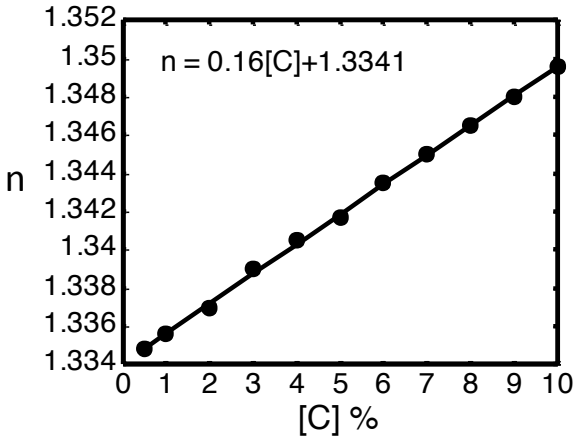

Fig. 8. Refractive index of dextrose at different concentrations and the linear regression fit. The relation between the refractive index and the concentration is obtained as $n = 0.16[C] + 1.334$.

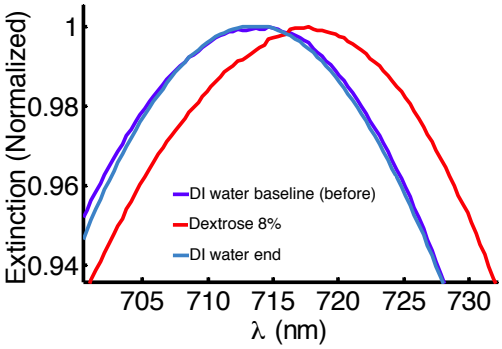

Fig. 9. The LSPR spectrum of a hybrid waveguide device consisting of $96 \times 57 \times 27$ *nm* gold nanorods integrated with a 865 *nm* $\times$ 200 *nm* Si_3N_4 waveguide for a dextrose solution of 8% concentration. The LSPR extinction spectrum of the device when DI water is flowing through the microfluidic channel is shown before and after the introduction of the dextrose solution, showing a good reversibility and stability over time.

#197900 - $15.00 USD Received 19 Sep 2013; revised 21 Nov 2013; accepted 27 Nov 2013; published 18 Dec 2013

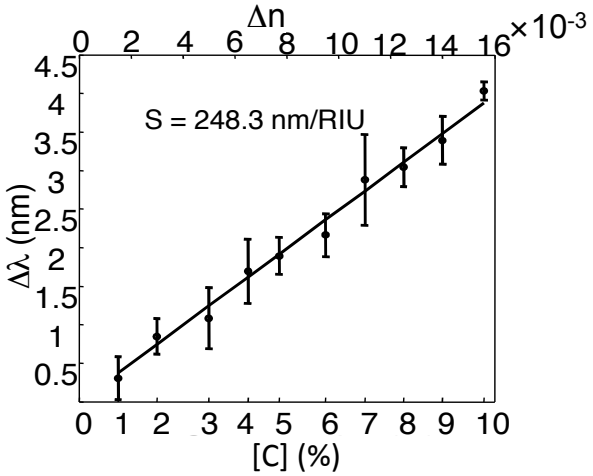

Fig. 10. The LSPR wavelength shift versus concentration for dextrose solutions of different concentrations. The hybrid waveguide device consists of a 865 $nm \times 200$ nm Si_3N_4 waveguide and $96 \times 57 \times 27$ nm gold nanorods. The linear regression fit to the measurement results suggests a large sensitivity of about 250 nm/RIU, with a coefficient of determination $R^2 = 0.988$.

Similar experiments are carried out for different concentrations of dextrose, and the results are shown in Fig. 10, where the LSPR wavelength shift is plotted versus concentration. We have also shown the refractive index of each solution obtained from our calibration data in Fig. 8. For each dextrose concentration, the measurement is repeated 10 times at different time intervals. The linear regression fit to the measurement data shows a sensitivity of about 250 nm/RIU. In these measurements, the coupling efficiency to the LSPR mode of the individual gold nanorod is 8.1% and the measured SNR is 24 dB. The detection limit in these measurements is limited to the resolution of the spectrometer (i. e., 0.3 nm.)

The large coupling efficiency, high sensitivity, and large SNR obtained here using a simple measurement system (i. e., a low-power broadband source and a simple spectrometer) makes the proposed hybrid waveguide structures good candidates for a broad range of applications including biomedical and environmental sensing. The proposed hybrid structure sensors can be used for multiplex sensing by fabricating an array of different nanoparticles on a single waveguide, each functionalized to bind to a specific target molecule.

5. Conclusion

Here we demonstrated a hybrid plasmonic-photonic-fluidic device with unique properties for on-chip sensing applications. The very small form factor, robust and alignment-insensitive architecture, large SNR, real-time response of the proposed device, large sensitivity, and its potential of integration with broadband light sources such as superluminescent light emitting diodes (SLEDs) and on-chip spectrometers [31, 32] makes it a practical candidate for lab-on-chip applications commensurate with the requirements of point-of-care diagnostics. The interrogation of single plasmonic nanoparticles in the proposed hybrid device with large SNR brings about new potentials for making ultracompact highly sensitive on-chip LSPR sensors. The integration of the hybrid on-chip LSPR sensor with microfluidics provides an efficient way of introducing the target analyte to the small interaction area in the vicinity of the plasmonic nanoparticles. An

#197900 - $15.00 USD Received 19 Sep 2013; revised 21 Nov 2013; accepted 27 Nov 2013; published 18 Dec 2013

array of the proposed hybrid structures can be implemented in parallel or in series for the detection of a panel of target molecules simultaneously. The idea of using hybrid plasmonic-photonic structures for on-chip LSPR sensing can also be extended to other waveguide platforms such as slot waveguides [33], hollow-core waveguides [34], and plasmonic waveguides [35].

Acknowledgments

This work was supported by the Defense Advanced Research Projects Agency (DARPA) under Contract HR 0011-10-1-0075 through the DARPA CIPHER Project.

#197900 - $15.00 USD Received 19 Sep 2013; revised 21 Nov 2013; accepted 27 Nov 2013; published 18 Dec 2013